

https://dspace.org/

About an (Im-)Possible Anomaly in Band Structure Theory

Quandt, Alexander

2022-09
Wiley
https://hdl.handle.net/10539/50062
Quandt, A. (2023), About an (Im-)Possible Anomaly in Band Structure Theory. Phys. Status Solidi B, 260: 2200049.

Downloaded from a DSpace repository. https://dspace.org/

physica status solidi b
www.pss-b.com

Check for updates

About an (Im-)Possible Anomaly in Band Structure Theory

Alexander Quandt

Based on an envelope function approach pioneered by Wannier and Slater, it can be shown that under the influence of strong effective magnetic fields in spinor space the band structure of certain materials gives rise to the analogs of tardyons and luxons, and in principle also to the analogs of tachyons. Such a (hypothetical) tachyonic band structure would be metallic, but with a gap in k-space and not in the range of allowed band energies $E_n(k)$. Some of the conditions to observe such a tachyonic anomaly in certain types of electronic band structures, which do not seem to be implausible, are discussed. Similar anomalies should appear in the spectrum of Landau levels. Furthermore, some of the pathologies that would come with such exotic band structure anomalies are pointed out.

1. Introduction

With the rise of topological insulators, it became clear that band structure theory, though being one of the oldest concepts in solid state physics, could still hold some surprises.[1] In his seminal work, Volovik had already pointed out that for certain solids, electrons in the vicinity of certain $\boldsymbol{k}$-points may behave like other types of elementary particles.[2]

In fact the linear dispersion relation of electrons around the corners of the reciprocal unit cell in graphene gives rise to physical properties, which are analogous to massless fermions.[3] However, it must be pointed out right from the beginning that the quasi-particle excitations around these special $\boldsymbol{k}$-points have only certain properties in common with real elementary particles, and therefore these quasi-particle excitations should never be confused with real or hypothetical elementary particles like neutrinos or magnetic monopoles.[2]

In Section 2, we will show that some of the peculiar behavior of band electrons around certain $\boldsymbol{k}$-points, and thus the resulting analogies to elementary particles, can easily be understood with the help of an envelope function approach pioneered by Wannier and Slater.[4,5] In the past, this approach has been used quite extensively to describe impurities in solids as analogs to hydrogen-like atoms.[6]

In Section 3, we will apply the envelope function approach to graphene-like systems. We will see, that his approach leads to a spinor description of the corresponding electronic states, but without the need to actually postulate anything. Furthermore, we will also point out the clear limitations of the envelope function approach, which entail limitations for the validity of the spinor picture of graphene-like bands. Unfortunately, these limitations are not always respected when setting up model Hamiltonians in the corresponding literature.

Another interesting aspect of applying the envelope function approach to graphene-like systems is the occurrence of three fundamental types of electronic band structures, which show analogies to very fundamental particles. As a tribute to a highly influential, but also highly debated article by Bilaniuk and Sudarshan, we call these band structures luxonic bands, tardyonic band, and tachyonic bands.[7]

In Section 4, we will discuss possible realizations of these fundamental types of band structures and we will use realistic data to predict some of the expected experimental results. It will be obvious that luxonic and tardyonic band structures have already been described quite extensively in the past, but without identifying them as such. To show the existence of tachyonic band structures would be a primer, and we hope that in Section 4, we may give some useful guiding lines for the necessary experimental studies of the corresponding band structure anomalies.

In Section 5, we point out similar anomalies for electrons in strong magnetic fields, based on the theory of Landau levels in graphene and other 2D materials. Those results emphasize again the importance of the envelope function approach. The latter allows for a direct inclusion of magnetic fields via the corresponding vector potentials, which reproduces all the known results, but also leads to some rather surprising novel predictions.

We will close our discussion in Section 6 with a short summary of our main results. Finally, in Section 7 we give a brief methodological description of the envelope function approach, and we explicitly calculate winding numbers, which characterize certain topological phase transitions discussed in Section 4.

2. The Envelope Function Approach

Let us briefly review the main features of the envelope function approach.[4,5] Our discussion will make it clear, why some analogies to elementary particles occasionally occur in band structure theory, and what these analogies actually mean.

A. Quandt
School of Physics
University of the Witwatersrand
Private Bag 3, 2050 Johannesburg, South Africa
E-mail: alex.quandt@wits.ac.za

The ORCID identification number(s) for the author(s) of this article can be found under https://doi.org/10.1002/pssb.202200049.

© 2022 The Authors. physica status solidi (b) basic solid state physics published by Wiley-VCH GmbH. This is an open access article under the terms of the Creative Commons Attribution License, which permits use, distribution and reproduction in any medium, provided the original work is properly cited.

DOI: 10.1002/pssb.202200049

© 2022 The Authors. physica status solidi (b) basic solid state physics published by Wiley-VCH GmbH

It is well known that in a perfectly periodic solid the electrons are described by Bloch states $\psi_{n,\boldsymbol{k}}(\boldsymbol{r})$, which are the eigenstates of a lattice periodic one-electron Hamiltonian $H(\boldsymbol{r})$ according to

$$H(\boldsymbol{r})\psi_{n,\boldsymbol{k}}(\boldsymbol{r}) = E_n(\boldsymbol{k})\psi_{n,\boldsymbol{k}}(\boldsymbol{r}) \tag{1}$$

Here the label n is the so-called band index, and the wave vectors $\boldsymbol{k}$ are from the first Brillouin zone. The eigenvalues $E_n(\boldsymbol{k})$ constitute the electronic band structure of the solid. Under translation by a lattice vector $\boldsymbol{R}$ the Bloch states $\psi_{n,\boldsymbol{k}}(\boldsymbol{r})$ are picking up a phase

$$\psi_{n,\boldsymbol{k}}(\boldsymbol{r}+\boldsymbol{R}) = e^{i\boldsymbol{k}\cdot\boldsymbol{R}}\psi_{n,\boldsymbol{k}}(\boldsymbol{r}) \tag{2}$$

Next, we apply a slowly varying external field $V(\boldsymbol{r})$ to this system, which could be a magnetic or electric field.[8] Furthermore, we want to approximate the band structure of the new Hamiltonian $H(\boldsymbol{r}) + V(\boldsymbol{r})$ in the vicinity of a given point $\boldsymbol{K}$ in $\boldsymbol{k}$-space (reciprocal space). Depending on the nature of the perturbation $V(\boldsymbol{r})$, the resulting eigenvalue problem does not necessarily involve a lattice periodic Hamiltonian anymore, and therefore we generally denote the new eigenvalue problem by

$$(H(\boldsymbol{r}) + V(\boldsymbol{r}))\Psi_n(\boldsymbol{r}) = \tilde{E}_n\Psi_n(\boldsymbol{r}) \tag{3}$$

It was first shown by Wannier that around a point $\boldsymbol{K}$ in the first Brillouin zone, the wave function $\Psi_n(\boldsymbol{r})$ can be approximated by the product $\Psi_n(\boldsymbol{r}) \approx \varphi_n(\boldsymbol{r})\psi_{n,\boldsymbol{K}}(\boldsymbol{r})$, where $\psi_{n,\boldsymbol{K}}(\boldsymbol{r})$ is the unperturbed Bloch state at point $\boldsymbol{K}$, and $\varphi_n(\boldsymbol{r})$ is an envelope function.[4] Furthermore, there arises a new eigenvalue problem to determine the eigenvalues $\tilde{E}_n$, which involves the envelope functions $\varphi_n(\boldsymbol{r})$, only. As explicitly shown by Slater the new eigenvalue problem is[5]

$$(E_n(\boldsymbol{K} - i\boldsymbol{\nabla}) + V(\boldsymbol{r}))\varphi_n(\boldsymbol{r}) = \tilde{E}_n\varphi_n(\boldsymbol{r}) \tag{4}$$

To determine the envelope functions $\varphi_n(\boldsymbol{r})$ locally around $\boldsymbol{K}$, the dispersion relation $E_n(\boldsymbol{k})$ obviously has to be substituted by a differential operator $E_n(\boldsymbol{K} - i\boldsymbol{\nabla})$. This is the essence of Wannier's theorem.[5]

It is on the basis of Wannier's theorem that possible analogies to elementary particles may eventually arise: Note that depending on the nature of the band structure $E_n(\boldsymbol{k})$ in the vicinity of point $\boldsymbol{K}$, the eigenvalue problem of Equation (4) for the envelope function $\varphi_n(\boldsymbol{r})$ may involve a Hamiltonian with a differential operator $E_n(\boldsymbol{K} - i\boldsymbol{\nabla})$ and a slowly varying perturbation $V(\boldsymbol{r})$, which is the same as the Hamiltonian of an elementary particle.

3. Fundamental Analogies: Luxons, Tardyons, and Tachyons

To discuss some interesting physics, let us now apply the envelope function approach to a graphene-like model system, which is described by a two-band model with the following 2D dispersion relation

$$E_{\pm}(k_x, k_y) = \pm t \cdot |e^{ik_y a} + 2e^{-ik_y a/2} \cdot \cos(\sqrt{3}k_x a/2)| \tag{5}$$

The corresponding schematic band structure with arbitrary values for the band parameters t and a is shown in **Figure 1**. We notice a linear dispersion relation around certain $\boldsymbol{k}$-points. These points are located at the corners of the reciprocal unit cell, and they are usually labeled by $\boldsymbol{K}'$. It is well known that the linear dispersion relation of points $\boldsymbol{k} = \boldsymbol{K} + \boldsymbol{g}$ in the vicinity of the point $\boldsymbol{K}$ at the corner of the reciprocal unit cell is approximately given by[9,10]

$$E_{\pm}(g_x, g_y) \approx \pm\hbar v_F g = \pm\hbar v_F\sqrt{g_x^2 + g_y^2} \tag{6}$$

Here the term v_F denotes the so-called Fermi velocity, which is related to the band parameters of Equation (5) by $v_F = \frac{3}{2}\frac{t\cdot a}{\hbar}$.

If we perturb this system by a slowly varying potential $V(\boldsymbol{r})$, we can apply Wannier's theorem to obtain some very interesting results in the vicinity of point $\boldsymbol{K}$. To this end, one has to make the substitutions $g_x \to -i\nabla_x$, $g_y \to -i\nabla_y$ in Equation (6), which leaves us with the problem of finding the square root of a differential operator $\sqrt{-(\nabla_x^2 + \nabla_y^2)}$. This boils down to a problem that has already been solved in a more general context by Dirac.[11] But in the present case, it is sufficient to note that[12]

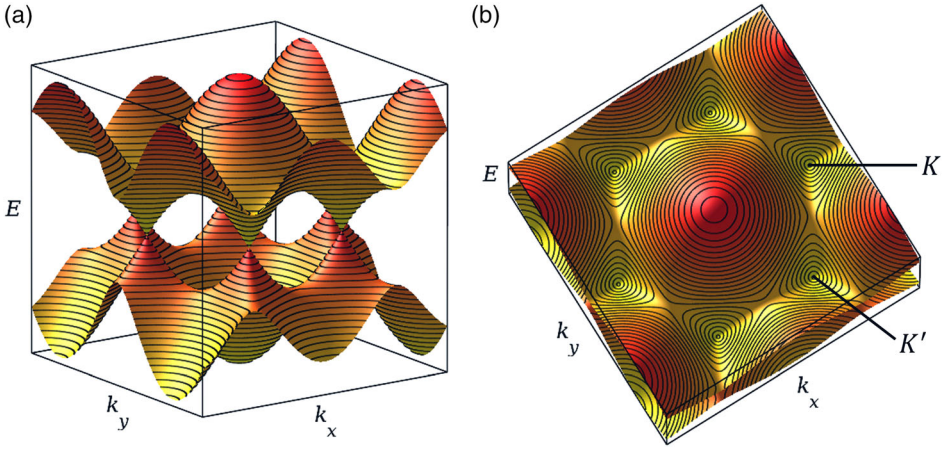


Figure 1. a) Band structure of a graphene-like system in the repeated zone scheme. b) The band structure is characterized by a linear dispersion relation around two special $\boldsymbol{k}$-points labeled K and K'.

© 2022 The Authors. physica status solidi (b) basic solid state physics published by Wiley-VCH GmbH

15213951, 2023, 1, Downloaded from https://onlinelibrary.wiley.com/doi/10.1002/pssb.202200049 by University Of Witwatersrand, Wiley Online Library on [16/09/2026]. See the Terms and Conditions (https://onlinelibrary.wiley.com/terms-and-conditions) on Wiley Online Library for rules of use; OA articles are governed by the applicable Creative Commons License

$$(\boldsymbol{a}\cdot\boldsymbol{\sigma})(\boldsymbol{b}\cdot\boldsymbol{\sigma}) = (\boldsymbol{a}\cdot\boldsymbol{b})I + i(\boldsymbol{a}\times\boldsymbol{b})\cdot\boldsymbol{\sigma} \tag{7}$$

where $\boldsymbol{a}$ and $\boldsymbol{b}$ are 3-vectors, and the 3-vector $\boldsymbol{\sigma}$ consists of the Pauli matrices σ_x, σ_y, and σ_z. The symbol I denotes a 2×2 unit matrix. Also, note that in the special case of the differential operator $\sqrt{-\left(\nabla_x^2+\nabla_y^2\right)}$, we actually have to set $a_z = b_z = 0$, while $a_x = b_x = -i\nabla_x$ and $a_y = b_y = -i\nabla_y$. Then the right-hand side of Equation (7) reproduces the radicand of Equation (6) twice as the two diagonal elements of a diagonal 2×2 matrix in spinor space, and the formal square root will correspond to the operator $(\boldsymbol{a}\cdot\boldsymbol{\sigma})$ on the left-hand side of Equation (7).

Thus, to take the formal square root of the differential operator related to Equation (6), one must automatically resort to a spinor picture, which has been largely popularized in the literature about graphene.[3] With all the substitutions related to the spinor approach made in Equation (6), one can again use the envelope function approach to arrive at a new eigenvalue problem, which is

$$H(x,y)\varphi_\pm(x,y) = (\hbar v_F\boldsymbol{\sigma}\cdot i\boldsymbol{\nabla})\varphi_\pm(x,y) = E_\pm\varphi_\pm(x,y) \tag{8}$$

Here $\varphi_\pm(x,y)$ is a spinor wave function. Again, it must be pointed out that this spinor picture is only an analogy to real elementary particles like neutrinos. In reality, the electrons in graphene move with Fermi velocity v_F, which is much smaller than the velocity of light c at which the neutrinos are moving. Such apparent discrepancies are always a warning sign that some of the analogies, which follow from the application of Wannier's theorem, must be taken with a grain of salt.[10]

Let us point out yet another important analogy. Just recall that terms like $-i\hbar\nabla_x$ may also be understood as momentum operators p_x in quantum mechanics, which means that after applying Wannier's theorem, we can also say that we have effectively substituted $\hbar g_x$ by a momentum operator p_x. Let us now square the expressions for the energies in Equation (6), and after carrying out these new substitutions we obtain the following expression

$$\left(E_\pm\left(g_x,g_y\right)\right)^2 = v_F^2\left(p_x^2+p_y^2\right) = v_F^2\boldsymbol{p}^2 \tag{9}$$

This is where things become very interesting. In their rather influential, but also highly debated article, Bilaniuk and Sudarshan suggested a general classification of elementary particles according to their energy–momentum relations.[7] Those are

$$\begin{aligned} E^2-\boldsymbol{p}^2c^2 &= m_0^2c^4 \quad \text{(tardyons)}\\ E^2-\boldsymbol{p}^2c^2 &= 0 \quad \text{(luxons)}\\ E^2-\boldsymbol{p}^2c^2 &= -m_*^2c^4 \quad \text{(tachyons)} \end{aligned} \tag{10}$$

The energy–momentum relations (i.e., dispersion relations) for these three classes of particles are shown in **Figure 2**. Note that the term m_0 stands the rest mass of the tardyons, and m_* is the absolute value of the imaginary rest mass $m_0 = im_*$ of the tachyons, which Bilaniuk and Sudarshan called the *meta*-mass of the tachyons.[7] It is obvious that the tardyons have an energy gap of size $2m_0c^2$, which means that even for vanishing momentum $\boldsymbol{p}$ there are two energy values $E_\pm = \pm m_0c^2$. The luxons with vanishing rest mass m_0 do not have an energy gap. The

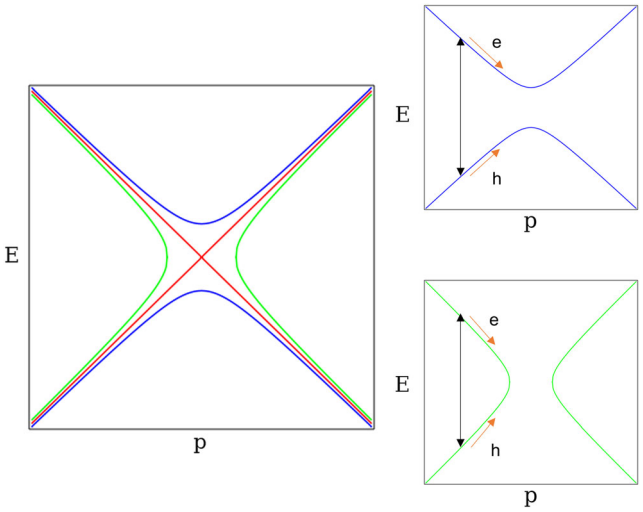


Figure 2. Left: Energy–momentum relations for tardyons (blue), luxons (red), and tachyons (green). More details can be found in the paper by Bilaniuk and Sudarshan.[7] Right: Optical excitation and subsequent thermalization of electrons and holes in a tardyonic band structure (top) and in a tachyonic band structure (bottom).

case of the tachyons is rather peculiar: as E^2 cannot be smaller than zero (because particles with imaginary energy will vanish in time), there are regions in momentum space that are obviously excluded. This leads to a gap in momentum space and not to an energy gap.

It is those peculiarities in the dispersion relations, which are the main topic of this article, and not so much the branding of prototype band structures in terms of tardyons, tachyons, and luxons. In the following sections, we will introduce a general theoretical framework to include those effects in a realistic description of certain 2D materials, which leads to interesting band structures and surprising results, which could be confirmed experimentally.

4. Band Structure Analogies of Luxons, Tardyons, and Tachyons

Let us now discuss how these concepts can be transferred into band structure theory. If we compare Equation (9) and (10), then we see that the dispersion relation in Equation (9) is the analog of a luxon with Fermi velocity v_F instead of light velocity c. The corresponding band structure is marked by a Dirac cone around $\boldsymbol{K}$, which is shown in **Figure 3**b. A typical case for such a solid is graphene.[3]

To find analogs of tardyons and tachyons, we introduce a self-energy term as a slowly varying perturbation of Zeeman-type in spinor space, which is

$$V(x,y) = \sigma_z(\alpha+i\beta) \tag{11}$$

In such an approach, the electrons are effectively modeled as quasi-particles, which are subject to complex many-body interactions. Let us also assume that $\beta = -\frac{\hbar}{\tau}$, where τ is the intrinsic

© 2022 The Authors. physica status solidi (b) basic solid state physics published by Wiley-VCH GmbH

15213951, 2023, 1, Downloaded from https://onlinelibrary.wiley.com/doi/10.1002/pssb.202200049 by University Of Witwatersrand, Wiley Online Library on [16/09/2026]. See the Terms and Conditions (https://onlinelibrary.wiley.com/terms-and-conditions) on Wiley Online Library for rules of use; OA articles are governed by the applicable Creative Commons License

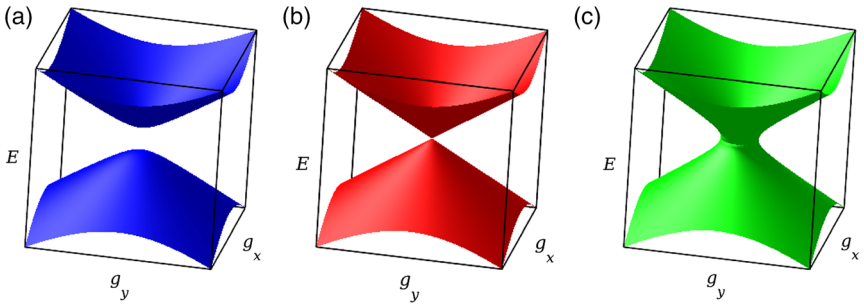


Figure 3. 2D band structures around point ***K***, which are the analogs of: a) tardyons with an energy gap, b) luxons without an energy gap, c) tachyons without an energy gap, but with a gap in ***k***-space.

quasi-particle lifetime of those many-body excitations (the minus sign implies causality). The term α is not supposed to be the corresponding real part of the self-energy, but it may also include an additional real potential, which can be externally controlled to modify α, up to the point where this term may even vanish.

It must be pointed out that for a typical quasi-particle with a complex self-energy, we obtain complex eigenvalues over ***k***-space, where the imaginary parts correspond to a broadening of the corresponding band structure. In contrast, for an ideal band electron subject to real potentials, we would not observe such a broadening.[10] We will see in the following that in the special case of vanishing real part α, which corresponds to the occurrence of tachyonic band structures, we would observe real eigenvalues over a large part of ***k***-space. So even in this rather exotic case of a tachyonic band structure, we may assume that there is no broadening of those bands, which would make the tachyonic bandgap observable, rather than being smeared out by a broadening of order $\frac{\hbar}{\tau}$. However, as pointed out before, the suggested effects will depend on the compensation of the real part of the self-energy by an applied external field, which might become a challenge for experimental studies.

Furthermore, as the spinor picture is only an analogy, the potential $V(x,y)$ does not involve a real or complex magnetic field, despite being of Zeeman type. Nevertheless, it might be interesting to note, that in the case of graphene, homogenous strain is the most likely analog of a magnetic field in this spinor picture.[13] The equivalent magnetic fields can be quite substantial in this case.[14] This will become more relevant in Section 5, where we discuss the spectrum of Landau levels in certain graphene-like systems.

After adding the Zeeman-like perturbation $V(x,y)$ to the model Hamiltonian $H(x,y)$ we obtain a new eigenvalue problem

$$\begin{aligned}(H(x,y)+V(x,y))\varphi_{\pm}(x,y) &= (\hbar v_F \boldsymbol{\sigma}\cdot i\boldsymbol{\nabla} + (\alpha+i\beta)\sigma_z)\varphi_{\pm}(x,y)\\ &= E_{\pm}\varphi_{\pm}(x,y)\end{aligned} \tag{12}$$

The corresponding eigenvalues in the vicinity of ***K*** are

$$E_{\pm}(g_x,g_y) \approx \pm\sqrt{v_F^2(\hbar^2 g_x^2+\hbar^2 g_y^2)+(\alpha+i\beta)^2} \tag{13}$$

At this point, it makes sense to invoke some of the mathematical concepts, which the author has illustrated in a recent publication.[15] The radicand in Equation (13) is actually a discriminant D (up to an irrelevant factor of 4) with $D=(E_+-E_-)^2$. If D were real, then we could easily classify the spectrum of the perturbed Hamiltonian, with two real eigenvalues for $D>0$, two degenerate states for $D=0$, and a pair of complex conjugate eigenvalues for $D<0$. One can easily check that D falls under this category for $(\alpha\neq 0,\beta=0)$, $(\alpha=0,\beta\neq 0)$, and $(\alpha=0,\beta=0)$.

The latter leads to a dispersion relation, which comes in the shape of a Dirac cone around point ***K***, and which is shown in Figure 3b. This is the typical band structure found in materials like graphene. When we compare those results to the results of Equation (10), we see that this type of band structure corresponds to a luxon.

Likewise, we see that the case with $\alpha\neq 0,\beta=0$ has the energy–momentum relation of a tardyon, with an energy gap of size $\alpha\equiv 2m_0v_F^2$ and with a rest mass parameter m_0. In Figure 3a, we show a typical tardyonic gapped band structure, which is found around point ***K*** in h-BN. This type of model Hamiltonian is often used in the field of topological insulators, where it describes gapped phases like hexagonal BN.[1] Then the topological phase transition occurs between the two gapped phases with $\alpha>0$ and $\alpha<0$ at a critical point with $\alpha=0$, where the gap in the band structure closes at $\boldsymbol{g}=0$. This topological phase transition involves a change in the sign of the winding numbers which characterize those gapped phases, and it seems unavoidable that such a transition will involve a gapless critical point. However, this will no longer be the case when $\beta\neq 0$, as was already pointed out previously in a more general context.[15]

Let us, therefore, discuss the more exotic case of a tachyonic band structure, which is the case with $\alpha=0,\beta\neq 0$.

With the substitution $\beta\equiv m_*v_F^2$, we obtain the following eigenvalue equation in the vicinity of point ***K***

$$\begin{aligned}(H(x,y)+V(x,y))\varphi_{\pm}(x,y) &= \left(\hbar v_F\boldsymbol{\sigma}\cdot i\boldsymbol{\nabla} + im_*v_F^2\sigma_z\right)\varphi_{\pm}(x,y)\\ &= E_{\pm}\varphi_{\pm}(x,y)\end{aligned} \tag{14}$$

The corresponding eigenvalues are

$$E_{\pm}(g_x,g_y) \approx \pm\sqrt{v_F^2(\hbar^2 g_x^2+\hbar^2 g_y^2)-m_*^2v_F^4} \tag{15}$$

which is the equivalent of the tachyonic dispersion relation described in Equation (10). We notice that for small enough

© 2022 The Authors. physica status solidi (b) basic solid state physics published by Wiley-VCH GmbH

15213951, 2023, 1, Downloaded from https://onlinelibrary.wiley.com/doi/10.1002/pssb.202200049 by University Of Witwatersrand, Wiley Online Library on [16/09/2026]. See the Terms and Conditions (https://onlinelibrary.wiley.com/terms-and-conditions) on Wiley Online Library for rules of use; OA articles are governed by the applicable Creative Commons License

values of g_x and g_y, there are no corresponding real energy values. This gap in $\boldsymbol{g}$-space leads to a band structure, which is a hyperboloid with a hole around $\boldsymbol{K}$, and this type of band structure is shown in Figure 3c. It might be worth noting that this tachyonic band structure shows some similarities to the isofrequency surfaces of hyperbolic metamaterials.[16,17] This analogy becomes clear when we identify the band energies $E_\pm$ with the range of allowed $\boldsymbol{k}_z$ vectors in a hyperbolic metamaterial, and the fixed term referring to the imaginary tachyon mass can be identified with the fixed frequency of an isofrequency surface for a hyperbolic metamaterial. Furthermore, analogies to hyperbolic metamaterials were previously pointed out for a system, which is similar to our present settings, and which consists of graphene nanoribbons modulated by an externally applied step-like electrostatic field.[18]

Please note that for the tachyonic band structure shown in Figure 3c, the group velocity $\boldsymbol{v}_g = \frac{\partial E(\boldsymbol{g})}{\partial \boldsymbol{g}}$ will go to infinity close to the gap in $\boldsymbol{g}$-space. As electrons are massive particles and surely bound by the speed of light, we should not expect to be able to resolve this band structure all the way to the bandgap. However, the optical excitation of electron–hole pairs away from the bandgap and the thermalization of the resulting free charge carriers through interactions with photons would lead to an increase in drift velocity, rather than to a decrease in drift velocity like for standard (tardyonic) systems. This effect is illustrated by the two insets on the right-hand side of Figure 2, and it could be used to demonstrate the presence of tachyonic electronic bands.

This brings us also to the following question: how realistic are these analogies of tardyons, luxons, and tachyons? We have already seen that typical analogs of tardyons and luxons exist in h-BN and graphene, and many more candidate materials exist in the field of topological insulators.[1] What about the tachyons? To guess the occurrence of gaps in $\boldsymbol{g}$-space for a tachyonic band structure, we rewrite Equation (15) using the relation $m_* v_F^2 = \beta = \frac{-\hbar}{\tau}$ and obtain

$$E_\pm(g_x, g_y) \approx \pm\hbar\sqrt{v_F^2 g^2 - \left(\frac{1}{\tau}\right)^2} \tag{16}$$

Thus, the expected anomalies around point $\boldsymbol{K}$ should occur whenever $|v_F g| < |\frac{1}{\tau}|$. For typical lattice constants of the order of $1nm$ the absolute value of the largest $\boldsymbol{g}$-vectors in the first BZ is of the order $g \approx 10^9\ \mathrm{m}^{-1}$ and smaller. A typical Fermi velocity like in graphene is of the order $v_F \approx 10^5 - 10^6\ \mathrm{m\ s}^{-1}$.[3] This means that locally, the product $v_F \cdot g$ could be of the order $v_F \cdot g \approx 10^{14}\ \mathrm{s}^{-1}$ or even smaller, and this would restrict the quasi-particle lifetimes τ to 10^{-14} s or less. Of course, materials with smaller Fermi velocities could show the same effects for larger quasi-particle lifetimes and probably for a smaller range of $\boldsymbol{g}$-vectors.

The most interesting aspect might be the following physical interpretation of those results: Despite the fact, that we started with a quasi-particle theory marked by a characteristic lifetime τ, we nevertheless obtain a band structure, which has stationary states in terms of real eigenvalues. Thus, it seems as if the stable tachyonic band structure may somehow be "driven" by short-lived many-body excitations.

Another interesting theoretical aspect of the present results leads us back to topological phase transitions. Instead of the general Zeeman-type perturbation in Equation (13), let us have a look at the following interaction

$$V(x, y) = \sigma_z e^{-i\varphi}\alpha \tag{17}$$

From a mathematical point of view, this corresponds to a standard operation in the complex plane, for which the term *twirl* has appropriately been chosen by Conway and Guy.[19] The twirl of Equation (17) is just a clockwise rotation, which will take us from a gapped (tardyonic) phase at $\varphi = 0$ over a gapped (tachyonic) phase at $\varphi = \frac{\pi}{2}$ to a third gapped (tardyonic) phase at $\varphi = \pi$, but without ever encountering the gapless critical point with $\alpha = 0$. This is a behavior, which should be generic for systems that involve quasi-particles.[15] Multiplications with arbitrary combinations of complex numbers would make the twirls in the interaction of Equation (17) even more interesting, and those twirls could still combine the three gapped phases marked by real eigenvalues, but totally avoid the gapless critical point.

Let us finally point out, that a strong hint for the existence of those fundamental band structures and particle analogs comes from optics. In suitably designed optical waveguide arrays one can use the analogy between discrete versions of the Dirac Hamiltonians described in this paper, and the paraxial Helmholtz equation in combination with coupled-mode theory.[20] This allows for the study of optical systems that behave like a Dirac Hamiltonian.[21] In this context, it is also possible to implement the equivalent of imaginary masses, and therefore the corresponding optical equivalents of tardyons, luxons, and tachyons have indeed been fabricated and studied.[22]

5. Electrons in Strong Magnetic Fields

Despite the introduction of a Zeeman-like interaction in Equation (11), we have not really included any magnetic fields up to now. This stems from the fact, that magnetic fields applied to quasi-2D systems like graphite and graphene lead to a Landau quantization of electronic states.[23–25] And they also lead to the occurrence of related effects like the quantum Hall effect at room temperature.[26,27] Their descriptions definitely go beyond a simple Zeeman-type of interaction.

At this point, it might not come as a big surprise anymore that the main results for an applied magnetic field can be neatly derived using the envelope function approach, which is based on early work by Luttinger.[8] The main result is the following: in the envelope function approach, just include magnetic fields by making the usual substitution in the momentum $\boldsymbol{p} \to \boldsymbol{p} + e\boldsymbol{A}$, using an appropriate vector potential $\boldsymbol{A}$. There will be no other terms and modifications.

In the present case of 2D systems, we just make the substitution in the basic Hamiltonian $H(\boldsymbol{r}) = -\hbar v_F \boldsymbol{\sigma}\cdot\boldsymbol{p} \to H(\boldsymbol{r}) = -\hbar v_F \boldsymbol{\sigma}\cdot(\boldsymbol{p} + e\boldsymbol{A})$ (see Equation 8). Let us choose the usual Landau gauge $\boldsymbol{A} = (-By, 0, 0)$, which obviously leads to a magnetic field $\boldsymbol{B}$ pointing in the z-direction. And let us explicitly write out the wave function $\varphi(x, y) = \begin{pmatrix}\varphi_1 \\ \varphi_2\end{pmatrix}$ in spinor space. Furthermore, let us add the staggered complex interaction of

© 2022 The Authors. physica status solidi (b) basic solid state physics published by Wiley-VCH GmbH

15213951, 2023, 1, Downloaded from https://onlinelibrary.wiley.com/doi/10.1002/pssb.202200049 by University Of Witwatersrand, Wiley Online Library on [16/09/2026]. See the Terms and Conditions (https://onlinelibrary.wiley.com/terms-and-conditions) on Wiley Online Library for rules of use; OA articles are governed by the applicable Creative Commons License

Equation (11). This leads to the following eigenvalue problem in spinor space

$$-v_F\begin{pmatrix}\alpha+i\beta & \left[-i\hbar\frac{\partial}{\partial x}-eBy\right]-\hbar\frac{\partial}{\partial y}\\ \left[-i\hbar\frac{\partial}{\partial x}-eBy\right]+\hbar\frac{\partial}{\partial y} & -(\alpha+i\beta)\end{pmatrix}\begin{pmatrix}\varphi_1\\ \varphi_2\end{pmatrix} = E\begin{pmatrix}\varphi_1\\ \varphi_2\end{pmatrix} \tag{18}$$

If we solve the corresponding linear system of equations for the spinor component φ_2, we obtain

$$\{E^2-(\alpha+i\beta)^2\}\varphi_2 = v_F^2\left(-\hbar^2\frac{\partial^2}{\partial y^2}+\left(-i\hbar\frac{\partial}{\partial x}-eBy\right)^2-\hbar eB\right)\varphi_2 \tag{19}$$

The first two terms in the large bracket on the right-hand side of this equation, when divided by $2m$ (m being the electron mass), are forming the usual analog of the shifted harmonic oscillator Hamiltonian used in the standard Landau quantization. If the system would show an additional periodicity in the z-direction, then we would also observe parabolic bands along the z-direction in $\boldsymbol{k}$-space on top of the standard Landau quantization scheme. And we would remain within the realm of band structure theory, as the title of our study suggests.

The shifted harmonic oscillator Hamiltonian on the right-hand side of Equation (19) has eigenvalues $\hbar\omega_c\left(n+\frac{1}{2}\right)$, with integers $n\geq 0$ and the cyclotron frequency $\omega_c=\frac{eB}{m}$. Inserting this result into Equation (19) and rearranging some terms leads us to

$$(E^2-(\alpha+i\beta)^2) = 2mv_F^2\hbar\omega_c n \tag{20}$$

and to the eigenvalues for the spinor component $\varphi_2(n)$

$$E_\pm(n) = \pm\sqrt{(\alpha+i\beta)^2+2\hbar eBv_F^2 n} \tag{21}$$

We note that the Landau levels obviously come in pairs according to Equation (21).

Note that similar reasoning may be applied when we solve the linear system of equations for the spinor component $\varphi_1(n)$, where we obtain the eigenvalues

$$E_\pm(n) = \pm\sqrt{(\alpha+i\beta)^2+2\hbar eBv_F^2(n+1)} \tag{22}$$

The whole situation may be summarized by using Equation (21) for the spectrum of the Landau levels and by assuming, that the eigenstates for the n-th Landau levels $E_\pm(n)$ have the structure $\begin{pmatrix}\varphi_1(n-1)\\ \pm\varphi_2(n)\end{pmatrix}$, with $\varphi_1(-1)=0$.[3]

Similar to what we discussed in the previous section, we are only interested in real eigenvalues $E_\pm(n)$ in the present context, which leads us again to three interesting cases. The first case corresponds to $\alpha\neq 0,\beta=0$, which we labeled as tardyonic in the last section. For $\alpha=mv_F^2$ in particular, we obtain a 2D analog of the energy eigenvalues of a free relativistic electron in a homogeneous magnetic field, which were first derived by Rabi.[28] The corresponding eigenvalues are

$$E_\pm(n) = \pm\sqrt{(mv_F^2)^2+2\hbar eBv_F^2 n} \tag{23}$$

Equation (22) and its special case Equation (23) suggest again a fundamental analogy to tardyons, luxons, and tachyons, which was summarized in Equation (10). To this end, we may identify α with the rest energy of a tardyonic particle with a real rest mass, and $i\beta$ may be identified with the rest energy of a tachyonic particle with an imaginary rest mass.

Let us now have a look at the second case with $\alpha=0,\beta=0$, which was labeled as luxonic in the previous section. It reproduces the known results for graphene.[25] The corresponding eigenvalues are

$$E_\pm(n) = \pm\sqrt{2\hbar eBv_F^2 n} \tag{24}$$

The last case is $\beta\neq 0,\alpha=0$, which we labeled as tachyonic in the last section. With the usual assumption that $\beta=-\frac{\hbar}{\tau}$, we obtain the following eigenvalues

$$E_\pm(n) = \pm\sqrt{2\hbar eBv_F^2 n-\frac{\hbar^2}{\tau^2}} \tag{25}$$

Again, we may ask ourselves when the eigenvalues of Equation (25) are real, and therefore physically meaningful in the present context. It is clear that we should observe anomalies (i.e., the absence of Landau levels) when $2\hbar eBv_F^2 n<\frac{\hbar^2}{\tau^2}$, because then we will no longer have real eigenvalues. This is particularly true for the Landau level with $n=0$, which is obviously the level, which is most sensitive to the corresponding purely imaginary perturbations. In general, after inserting all the known constants as in the last section, we obtain the following result

$$1.3164\cdot 10^{-3}\left[\frac{B}{1\,\mathrm{T}}\right]n(\mathrm{eV})^2<\frac{\hbar^2}{\tau^2} \tag{26}$$

For a very strong magnetic field of magnitude $B=10\,\mathrm{T}$, we conclude that $\frac{\hbar}{\tau}$ must be of the order of $10^{-1}\,\mathrm{eV}$ to see some anomalies even for Landau levels with $n\neq 0$. With $\hbar=6.582\cdot 10^{-16}\,\mathrm{eV}\cdot\mathrm{s}$ that ratio is met by quasi-particle lifetimes of $\tau\approx 10^{-14}\,\mathrm{s}$, like the result that we obtained in the previous section. Strong magnetic fields of that magnitude are difficult to achieve from a practical point of view, but they are still within the range of the magnetic field strengths for the strongest known permanent magnets. Given a moderate magnetic field of $B=0.1\,\mathrm{T}$, which corresponds to magnetic field strengths encountered in a typical ferrite magnet, the ratio $\frac{\hbar}{\tau}$ must be of the order of $10^{-2}\,\mathrm{eV}$. Thus, the corresponding quasi-particle lifetimes must be longer than for the case of an applied magnetic field of magnitude 10 T, and in the case of an applied magnetic field of magnitude 0.1 T, those quasi-particle lifetimes would be around $\tau\approx 10^{-13}\,\mathrm{s}$.

To summarize, the "tachyonic" case of Landau levels is again anomalous due to the absence of certain levels, and again a possible physical interpretation of those results may be that they are driven by short-lived quasi-particle excitations. Let us finally point out other known results concerning non-Hermitian potentials in the context of Landau levels. First of all, non-Hermitian

© 2022 The Authors. physica status solidi (b) basic solid state physics published by Wiley-VCH GmbH

15213951, 2023, 1, Downloaded from https://onlinelibrary.wiley.com/doi/10.1002/pssb.202200049 by University Of Witwatersrand, Wiley Online Library on [16/09/2026]. See the Terms and Conditions (https://onlinelibrary.wiley.com/terms-and-conditions) on Wiley Online Library for rules of use; OA articles are governed by the applicable Creative Commons License

15213951, 2023, 1, Downloaded from https://onlinelibrary.wiley.com/doi/10.1002/pssb.202200049 by University Of Witwatersrand, Wiley Online Library on [16/09/2026]. See the Terms and Conditions (https://onlinelibrary.wiley.com/terms-and-conditions) on Wiley Online Library for rules of use; OA articles are governed by the applicable Creative Commons License

imaginary potentials have been discussed by Ramos and coworkers before in the framework of the classical Landau Hamiltonian, where these authors also point out the possibility, that such potentials can lead to real eigenvalues.[29] Hue and coworkers have examined Landau levels for non-Hermitian Hamiltonians with gain and loss.[30] Their study also comprises staggered interaction terms, which are quite similar to the present study. Although the major focus of their study was to establish the existence of Dirac cones for their model Hamiltonians, they also discuss the existence of Landau levels for their models, including the existence of a zero mode and related edge states. Another interesting implementation of non-Hermitian Hamiltonians in the context of Landau levels has been suggested by Zhang and Franz, who looked at Landau quantization in electrical circuits.[31] In contrast to our models, the non-Hermiticity of their model Hamiltonians refers to off-diagonal elements, but the existence of real eigenvalues is also noted in their study. Furthermore, Shen and Fu have studied Landau levels for systems with complex self-energy terms.[32] The focus of their study is on quantum oscillations in such systems, where they derive an analytic expression for the Landau levels, which is very similar to what we discussed in this Section. However, they do not mention the special case of tachyonic bands, and therefore they describe Landau levels for models with complex self-energy, but without discussing purely imaginary potentials.

6. Conclusion

In summary, we have discussed the application of Wannier's theorem to obtain the analogs of tardyons, luxons, and tachyons. We have seen that the equivalents of tardyons and luxons have already been studied quite intensively in solid-state physics. This is not the case for tachyonic band structures and related band structure anomalies, like the partial vanishing of Landau levels. And therefore, it might be worth designing and carrying out experiments in search of these anomalies, even with the danger of obtaining null results or impractical results.

With possible null results in mind, we caution the reader to take the present results with a grain of salt. We have already noticed that infinite group velocities at the edges of a bandgap in $\boldsymbol{k}$-space are a warning sign that a tachyonic envelope function suffers from the same sort of maladies, which are attributed to their hypothetical counterparts in particle physics.[7]

In the end one could say it with Murray Gell-Mann: "Anything that is not forbidden is compulsory." In that sense, the idea that there could be gaps in $\boldsymbol{k}$-space rather than energy gaps certainly contests our conventional ideas about band structures ("spaghetti diagrams") in solid-state physics, and the same physics would lead to certain anomalies in the spectrum of electronic states subject to an applied magnetic field.

7. Methods

In the following, we will give some background material concerning the envelope function approach used throughout this article. And we also illustrate the numerical and analytic determination of winding numbers for the types of topological phase transitions discussed in Section 4. We guess that this background material could also be useful to tackle other topics beyond the scope of our current discussion.

Brief Outline of the Envelope Function Approach

The basic ideas behind the envelope function approach go back to Wannier and Slater.[4,5] In Section 2, our major focus was on the application of Wannier's theorem, which was used as a justification to go from Equation (3) and (4), i.e., to go from the eigenvalue problem of a perturbed Bloch electron to an eigenvalue problem for its envelope function, which is valid in the vicinity of a given point $\boldsymbol{K}$ in reciprocal space.

In the following, we want to give more background information to justify the various instances, where we applied Wannier's theorem in Section 3–5. Let us start again from Equation (3), which is the eigenvalue problem for the perturbed Bloch electron:

$$(H(\boldsymbol{r}) + V(\boldsymbol{r}))\Psi_n(\boldsymbol{r}) = \tilde{E}_n\Psi_n(\boldsymbol{r})$$

Then we expand the wave function $\Psi_n(\boldsymbol{r})$ as follows

$$\Psi_n(\boldsymbol{r}) = \sum_{\boldsymbol{k}}\beta_{n,\boldsymbol{k}}\psi_{n,\boldsymbol{k}}(\boldsymbol{r}) \approx \varphi_n(\boldsymbol{r})\psi_{n,\boldsymbol{K}}(\boldsymbol{r}) \tag{27}$$

This is an exact expansion of the wave function into a complete set of Bloch states $\psi_{n,\boldsymbol{k}}(\boldsymbol{r})$, which can be approximated by the product $\Psi_n(\boldsymbol{r}) \approx \varphi_n(\boldsymbol{r})\psi_{n,\boldsymbol{K}}(\boldsymbol{r})$, where $\psi_{n,\boldsymbol{K}}(\boldsymbol{r})$ is the unperturbed Bloch state at a given point $\boldsymbol{K}$, and $\varphi_n(\boldsymbol{r})$ is an envelope function. Note that the envelope function is characterized by the following plane wave expansion

$$\varphi_n(\boldsymbol{r}) = \sum_{\boldsymbol{k}}\beta_{n,\boldsymbol{k}}e^{i(\boldsymbol{k}-\boldsymbol{K})\cdot\boldsymbol{r}} \tag{28}$$

where $\boldsymbol{k} = \boldsymbol{K} + \boldsymbol{g}$. Next, let us insert an exact expansion of the wave function $\Psi_n(\boldsymbol{r})$ into Equation (3) and sandwich with a Bloch state $\psi^*_{n,\boldsymbol{k}}(\boldsymbol{r})$, which leads to

$$E_n(\boldsymbol{k})\beta_{n,\boldsymbol{k}} + \sum_{\boldsymbol{k}'}\langle\psi_{n\boldsymbol{k}}|V|\psi_{n\boldsymbol{k}'}\rangle\beta_{n,\boldsymbol{k}'} = \tilde{E}_n\beta_{n,\boldsymbol{k}} \tag{29}$$

To arrive at an eigenvalue problem for the envelope function $\varphi_n(\boldsymbol{r})$, we multiply Equation (29) by $e^{i(\boldsymbol{k}-\boldsymbol{K})\cdot\boldsymbol{r}}$ and sum over $\boldsymbol{k}$. This leads to

$$\sum_{\boldsymbol{k}}E_n(\boldsymbol{k})\beta_{n,\boldsymbol{k}}e^{i(\boldsymbol{k}-\boldsymbol{K})\cdot\boldsymbol{r}} + \sum_{\boldsymbol{k}}\sum_{\boldsymbol{k}'}\langle\psi_{n\boldsymbol{k}}|V|\psi_{n\boldsymbol{k}'}\rangle e^{i(\boldsymbol{k}-\boldsymbol{K})\cdot\boldsymbol{r}}\beta_{n,\boldsymbol{k}'} = \tilde{E}_n\sum_{\boldsymbol{k}}\beta_{n,\boldsymbol{k}}e^{i(\boldsymbol{k}-\boldsymbol{K})\cdot\boldsymbol{r}} \tag{30}$$

With $\sum_{\boldsymbol{k}}\langle\psi_{n\boldsymbol{k}}|V|\psi_{n\boldsymbol{k}'}\rangle e^{i(\boldsymbol{k}-\boldsymbol{k}')\cdot\boldsymbol{r}} \approx V(\boldsymbol{r})$ for a slowly varying perturbing potential, Equation (30) will go over into one of the key results of the envelope function approach.

$$\sum_{\boldsymbol{k}}E_n(\boldsymbol{k})\beta_{n,\boldsymbol{k}}e^{i(\boldsymbol{k}-\boldsymbol{K})\cdot\boldsymbol{r}} + V(\boldsymbol{r})\varphi_n(\boldsymbol{r}) = \tilde{E}_n\varphi_n(\boldsymbol{r}) \tag{31}$$

To prove Wannier's theorem, we only have to make the assumption that, in the vicinity of a given point $\boldsymbol{K}$ in reciprocal space, we can find an analytic expansion of the dispersion relation $E_n(\boldsymbol{k}) \approx F_n(\boldsymbol{K}) + G_n(\boldsymbol{k}-\boldsymbol{K})$, where $\boldsymbol{g} = \boldsymbol{k} - \boldsymbol{K}$. We can

© 2022 The Authors. physica status solidi (b) basic solid state physics published by Wiley-VCH GmbH

finally rewrite Equation (31), based on very elementary results of Fourier theory[33]

$$F_n(\boldsymbol{K})\varphi_n(\boldsymbol{r}) + G_n(-i\boldsymbol{\nabla})\varphi_n(\boldsymbol{r}) + V(\boldsymbol{r})\varphi_n(\boldsymbol{r}) = \tilde{E}_n\varphi_n(\boldsymbol{r}) \tag{32}$$

This result is equivalent to the assumption that in any analytic expansion of $E_n(\boldsymbol{k})$ around a given point $\boldsymbol{K}$ in reciprocal space, we can substitute $\boldsymbol{g} = \boldsymbol{k} - \boldsymbol{K}$ by $-i\boldsymbol{\nabla}$, and then we let the resulting differential operator act on the envelope function $\varphi_n(\boldsymbol{r})$ to determine the corresponding eigenvalues.

A recent and more detailed discussion of the envelope function approach with interesting applications to the band structure of semiconductors can be found elsewhere.[34]

Winding Numbers of Model Hamiltonians

It was mentioned in Section 4 that the tardyonic band structure $E_{\pm}\left(g_x, g_y\right) = \pm\sqrt{v_F^2\left(\hbar^2 g_x^2 + \hbar^2 g_y^2\right) + \alpha^2}$ is marked by a topological phase transition, which refers to two tardyonic phases with $\alpha > 0$ and $\alpha < 0$. This topological phase transition goes over a critical point at $\alpha = 0$, which is marked by a gap closing at $\boldsymbol{g} = 0$. And it involves a change in the winding numbers, which characterize the gapped tardyonic phases.

Note that the winding numbers for similar types of band structures were discussed by the author in a recent publication and worked out numerically using MAPLE.[15] In the spirit of this article, we will briefly introduce the concept of winding numbers for a given model Hamiltonian, based on the vectorization of matrix Hamiltonians and on the corresponding Kronecker index.

Note that these types of winding numbers are only well-defined for a very restricted class of Hamiltonians, but one of the most interesting results is the fact that the determination of these types of winding numbers always leads to very fascinating integrals.[15] In fact, one of those fascinating integrals will become the central result of this subsection, where in addition to the numerical results obtained in our previous publication, we will also verify the validity of those numerical results in an analytic fashion. By doing so, we would like to warn the reader that our approach is elementary and only valid close to the topological phase transition, and most likely not very elegant from a mathematical point of view.

We start our discussion with the observation, that the Hamiltonian, which gives rise to the tardyonic bands, can be written as follows in spinor space.

$$\begin{aligned} H(g_x, g_y, \alpha) &= \begin{pmatrix} \alpha & -\hbar v_F\left(g_x - ig_y\right) \\ -\hbar v_F\left(g_x + ig_y\right) & -\alpha \end{pmatrix} \\ &\equiv \begin{pmatrix} h_z & h_x - ih_y \\ h_x + ih_y & -h_z \end{pmatrix} \end{aligned} \tag{33}$$

We can rewrite this Hamiltonian by expanding it into the basis of 2×2 matrices, which is provided by the Pauli matrices

$$H(g_x, g_y, \alpha) = H\left(h_x, h_y, h_z\right) = h_x\sigma_x + h_y\sigma_y + h_z\sigma_z \tag{34}$$

Based on such an expansion, we can introduce a vector $\boldsymbol{h} = \left(h_x, h_y, h_z\right)$ to represent this spinor Hamiltonian. Next, we map the vector $\boldsymbol{h}$ onto an ellipsoid in 3-space by introducing the following parametrization $\boldsymbol{h} = (k\sin\varphi_1\cos\varphi_2, k\sin\varphi_1\sin\varphi_2, m\cos\varphi_1)$, where k and m are related to the original parameters of the spinor Hamiltonian, and the new parameters, which are used to determine the winding numbers, span the intervals $\varphi_1\,\varepsilon\,[0,\pi]$ and $\varphi_2\,\varepsilon\,[0,2\pi]$, and thus effectively vary over a reference 2-sphere.

The winding number, which characterizes the movement of the vector $\boldsymbol{h}$ over the ellipsoid, is quantified by the Kronecker index[15,35]

$$\text{index}(\boldsymbol{h}) = \frac{1}{4\pi}\int_0^{2\pi}\int_0^{\pi}\frac{1}{||\boldsymbol{h}||^3}vol^3\left(\boldsymbol{h}, \frac{\partial\boldsymbol{h}}{\partial\varphi_1}, \frac{\partial\boldsymbol{h}}{\partial\varphi_2}\right)d\varphi_1 d\varphi_2 \tag{35}$$

A straightforward calculation based on the suggested parametrization for the vector $\boldsymbol{h}$ leads to a vector norm given by $||\boldsymbol{h}|| = \sqrt{k^2\sin^2\varphi_1 + m^2\cos^2\varphi_1}$, and the volume form boils down to working out a determinant according to $vol^3\left(\boldsymbol{h}, \frac{\partial\boldsymbol{h}}{\partial\varphi_1}, \frac{\partial\boldsymbol{h}}{\partial\varphi_2}\right) \equiv |\boldsymbol{h}, \frac{\partial\boldsymbol{h}}{\partial\varphi_1}, \frac{\partial\boldsymbol{h}}{\partial\varphi_2}| = k^2 m\sin\varphi_1$. Then the Kronecker index becomes

$$\text{index}(\boldsymbol{h}) = \frac{2\pi}{4\pi}\int_0^{\pi}\frac{k^2 m\sin\varphi_1}{(k^2\sin^2\varphi_1 + m^2\cos^2\varphi_1)^{\frac{3}{2}}}d\varphi_1 = \text{sign}(m) \tag{36}$$

It is fascinating to evaluate this integral numerically (e.g., using MAPLE) and to verify that for arbitrary choices of the parameters k and m, the integral and the corresponding winding number are only determined by the sign of the parameter m.

Based on our parametrization, changes in the sign of m are related to changes in the sign of α for a given parameter φ_1 and vice versa, and therefore the topological phase transitions between a phase with $\alpha > 0$ and a phase with $\alpha < 0$ are obviously marked by a change in their winding numbers, which is based on a suitably defined Kronecker index given by Equation (36).

Let us finally show how to work out the key integral of Equation (36) close to the topological phase transition. The first step consists of rewriting this integral

$$\int_0^{\pi}\frac{k^2 m\sin\varphi_1}{(k^2\sin^2\varphi_1 + m^2\cos^2\varphi_1)^{\frac{3}{2}}}d\varphi_1 = \int_{-1}^{1}\frac{a}{(1-(1-a^2)u^2)^{3/2}}du \tag{37}$$

where $a = \frac{m}{|k|}$ and $u = \cos\varphi_1$. In the following, we will always assume that $0 < (b = 1 - a^2) < 1$, which refers to special choices of k and m close to the phase transition, where m may always be supposed to be sufficiently small for a given $|k|$. From those assumptions, it immediately follows that $a = \text{sign}(a)\sqrt{1-b} = \text{sign}(m)\sqrt{1-b}$.

Next, we make use of the generalized binomial theorem

$$(x+y)^r = \sum_{k=0}\binom{r}{k}x^{r-k}y^k \tag{38}$$

© 2022 The Authors. physica status solidi (b) basic solid state physics published by Wiley-VCH GmbH

15213951, 2023, 1, Downloaded from https://onlinelibrary.wiley.com/doi/10.1002/pssb.202200049 by University Of Witwatersrand, Wiley Online Library on [16/09/2026]. See the Terms and Conditions (https://onlinelibrary.wiley.com/terms-and-conditions) on Wiley Online Library for rules of use; OA articles are governed by the applicable Creative Commons License

This expression leads to convergent series for $|x| > |y|$ and in particular for r being a rational number, which is the special case that we are interested in. Note that the binomial coefficients are directly related to the Gamma functions via[36]

$$\binom{r}{k} = \frac{\Gamma(r+1)}{\Gamma(r-k+1)\Gamma(k+1)} \tag{39}$$

From Equation (38) and (39), it follows that

$$\begin{aligned}
&\sqrt{1-b} = 1-\tfrac{1}{2}b-\tfrac{1}{8}b^2-\tfrac{1}{16}b^3+\ldots \quad (x=1, y=-b, r=\tfrac{1}{2})\\
&\tfrac{1}{\sqrt{1-b}} = 1+\tfrac{1}{2}b+\tfrac{3}{8}b^2+\tfrac{5}{16}b^3+\ldots \quad (x=1, y=-b, r=-\tfrac{1}{2})\\
&(1-bu^2)^{-3/2} = 1+\tfrac{3}{2}bu^2+\tfrac{15}{8}b^2u^4+\tfrac{35}{16}b^3u^6+\ldots (x=1, y=-bu^2, r=-\tfrac{3}{2})
\end{aligned} \tag{40}$$

where we have assumed that $|b| < 1$ and $|u| \leq 1$.

Rewriting the right-hand side of Equation (37), making use of the binomial expansions of Equation (40), and an elementary integration finally lead to

$$\begin{aligned}
&\operatorname{sign}(m)\sqrt{1-b}\cdot\int_{-1}^{1}(1-bu^2)^{-\frac{3}{2}}du\\
&= \operatorname{sign}(m)\sqrt{1-b}\cdot\left[2+b+\frac{6}{8}b^2+\frac{10}{16}b^3+\ldots\right]\\
&= \operatorname{sign}(m)\sqrt{1-b}\cdot\frac{2}{\sqrt{1-b}} = 2\operatorname{sign}(m)
\end{aligned} \tag{41}$$

which shows the validity of Equation (36) close to the topological phase transition.

Acknowledgements

The author would like to thank the Mandelstam Institute for Theoretical Physics (MITP) and the DST-NRF Centre of Excellence in Strong Materials (CoE-SM) at the University of the Witwatersrand for their support. The author also thanks the transcontinental ARUA Centre of Excellence in Materials, Energy and Nanotechnology (CoE-MEN) for support.

Conflict of Interest

The author declares no conflict of interest.

Data Availability Statement

Data sharing is not applicable to this article as no new data were created or analyzed in this study.

Keywords

band structure, Bloch state, envelope function, graphene, Landau quantization tachyon

Received: February 2, 2022
Revised: September 27, 2022
Published online: October 19, 2022

[1] M. Z. Hasan, C. L. Kane, *Rev. Mod. Phys.* **2010**, *82*, 3045.
[2] G. E. Volovik, *The Universe in a Helium Droplet*, Oxford University Press, Oxford, UK **2003**.
[3] A. H. Castro Neto, F. Guinea, N. M. R. Peres, K. S. Novoselov, A. K. Geim, *Rev. Mod. Phys.* **2009**, *81*, 109.
[4] G. H. Wannier, *Phys. Rev.* **1937**, *52*, 191.
[5] J. C. Slater, *Phys. Rev.* **1949**, *76*, 1592.
[6] O. Madelung, *Introduction to Solid-State Theory*, Springer, Berlin, Germany **1996**.
[7] O. M. Bilaniuk, E. C. G. Sudarshan, *Phys. Today* **1969**, *22*, 47.
[8] J. M. Luttinger, *Phys. Rev.* **1951**, *84*, 814.
[9] G. W. Semenoff, *Phys. Rev. Lett.* **1984**, *53*, 2449.
[10] G. D. Mahan, *Condensed Matter in a Nutshell*, Princeton University Press, Princeton, NJ **2011**.
[11] P. A. M. Dirac, *Proc. R. Soc. London A* **1928**, *117*, 610.
[12] M. Chaichian, R. Hagedorn, *Symmetries in Quantum Mechanics*, IOP Publishing, London, UK **1998**.
[13] F. Guinea, M. I. Katsnelson, A. K. Geim, *Nat. Phys.* **2010**, *6*, 30.
[14] N. Levy, S. A. Burke, K. L. Meaker, M. Panlasigui, A. Zettl, F. Guinea, A. H. Castro Neto, M. F. Crommie, *Science* **2010**, *329*, 544.
[15] A. Quandt, *Physica B* **2021**, *612*, 41286.
[16] P. Huo, S. Zhang, Y. Liang, Y. Lu, T. Xu, *Adv. Opt. Mater.* **2019**, *7*, 1801616.
[17] A. Aigner, J. M. Dawes, S. A. Maier, H. Ren, *Light: Sci. Appl.* **2022**, *11*, 9.
[18] M. G. Silveirinha, N. Engheta, *Phys. Rev. B* **2012**, *85*, 195413.
[19] J. H. Conway, R. K. Guy, *The Book of Numbers*, Springer, New York, NY **1996**.
[20] H. A. Haus, *Waves and Fields in Optoelectronics*, Prentice-Hall, Upper Saddle River, NJ **1984**.
[21] J. Zeuner, N. K. Efremidis, R. Kiel, F. Dreisov, D. Christodoulidis, A. Tümmermann, S. Nolte, A. Szameit, *Phys. Rev. Lett.* **2012**, *109*, 023602.
[22] A. Szameit, M. C. Rechtsman, O. Bahat-Treidel, M. Segev, *Phys. Rev. A* **2011**, *84*, 021806(R).
[23] G. Li, E. Y. Andrei, *Nat. Phys.* **2007**, *3*, 623.
[24] T. Matsui, H. Kambara, Y. Niimi, K. Tagami, M. Tsukada, H. Fukuyama, *Phys. Rev. Lett.* **2005**, *94*, 226403.
[25] L. J. Yin, K. K. Bai, W. X. Wang, S. Y. Li, Y. Zhang, L. He, *Fund. Phys.* **2017**, *12*, 127208.
[26] K. S. Novoselov, Z. Jiang, Y. Zhang, S. V. Morozov, H. L. Stoermer, U. Zeitler, J. C. Maan, G. S. Boebinger, P. Kim, A. K. Geim, *Science* **2007**, *315*, 1379.
[27] Y. Zhang, Y. W. Tan, H. L. Stoermer, P. Kim, *Nature* **2005**, *438*, 201.
[28] I. I. Rabi, *Z. Phys.* **1928**, *49*, 507.
[29] B. F. Ramos, I. A. Pedrosa, K. Bakke, *Int. J. Mod. Phys. A* **2019**, *34*, 1950072.
[30] H. Xue, Q. Wang, B. Zhang, Y. D. Chong, *Phys. Rev. Lett.* **2020**, *124*, 236403.
[31] X.-X. Zhang, M. Franz, *Phys. Rev. Lett.* **2020**, *124*, 046401.
[32] H. Shen, L. Fu, *Phys. Rev. Lett.* **2018**, *121*, 026403.
[33] R. S. Strichartz, *A Guide To Distribution Theory and Fourier Transforms*, World Scientific Publishing, Singapore, Singapore **2003**.
[34] E. Kaxiras, J. D. Joannopoulos, *Quantum Theory of Materials*, Cambridge University Press, Cambridge, UK **2019**.
[35] T. Frenkel, *The Geometry of Physics*, Cambridge University Press, Cambridge, UK **1997**.
[36] M. Abramowitz, I. A. Stegun, *Handbook of Mathematical Functions*, 9th ed., Dover Publications, New York, NY **1970**.

© 2022 The Authors. physica status solidi (b) basic solid state physics published by Wiley-VCH GmbH

15213951, 2023, 1, Downloaded from https://onlinelibrary.wiley.com/doi/10.1002/pssb.202200049 by University Of Witwatersrand, Wiley Online Library on [16/09/2026]. See the Terms and Conditions (https://onlinelibrary.wiley.com/terms-and-conditions) on Wiley Online Library for rules of use; OA articles are governed by the applicable Creative Commons License